HHS Public Access

Author manuscript

Acta Biomater. Author manuscript; available in PMC 2019 March 15.

Published in final edited form as:

Acta Biomater. 2018 March 15; 69: 342–351. doi:10.1016/j.actbio.2018.01.016.

Synergistic interplay between the two major bone minerals, hydroxyapatite and whitlockite nanoparticles, for osteogenic differentiation of mesenchymal stem cells

Hao Cheng[a,b], **Rosa Chabok**[a,b], **Xiaofei Guan**[a,b,c], **Aditya Chawla**[a,b,c], **Yuxiao Li**[a,b], **Ali Khademhosseini**[a,b,c,d,e,*], and **Hae Lin Jang**[a,b,c,*]

[a]Division of Engineering in Medicine, Department of Medicine, Biomaterials Innovation Research Center, Harvard Medical School, Brigham & Women's Hospital, Boston, MA 02139, USA

[b]Division of Health Sciences & Technology, Harvard-Massachusetts Institute of Technology, Massachusetts Institute of Technology, Cambridge, MA 02139, USA

[c]Wyss Institute for Biologically Inspired Engineering, Harvard University, Boston, MA 02115, USA

[d]Department of Bioindustrial Technologies, College of Animal Bioscience & Technology, Konkuk University, Seoul 143-701, Republic of Korea

[e]Department of Physics, King Abdulaziz University, Jeddah 21569, Saudi Arabia

Abstract

The inorganic part of human bone is mainly composed of hydroxyapatite (HAP: $Ca_{10}(PO_4)_6(OH)_2$) and whitlockite (WH: $Ca_{18}Mg_2(HPO_4)_2(PO_4)_{12}$) minerals, where the WH phase occupies up to 20-35% of total weight. These two bone minerals have different crystal structures and physicochemical properties, implying their distinguished role in bone physiology. However, until now, the biological significance of the presence of a certain ratio between HAP and WH in bone is unclear. To address this fundamental question, bone mimetic scaffolds are designed to encapsulate human mesenchymal stem cells (MSCs) for assessing their osteogenic activity depending on different ratios of HAP and WH. Interestingly, cellular growth and osteogenic differentiation are significantly promoted when MSCs are grown with a 3 to 1 ratio of HAP and WH nanoparticles, which is similar to bone. One of the reasons for this synergism between HAP and WH in hydrogel scaffolds is that, while WH nanoparticles can enhance osteogenic differentiation of MSCs compared to HAP, WH counterintuitively decreases the mechanical stiffness of nanocomposite hydrogels and hinders the osteogenic activity of cells. Taken together, these findings identify the optimal ratio between two major minerals in bone mimetic scaffolds to maximize the osteogenic differentiation of MSCs.

*Corresponding authors. alik@bwh.harvard.edu (A. Khademhosseini), hiang@bwh.harvard.edu (H.L. Jang).

Conflict of interest

Authors declare no conflict of interest.

Graphical abstract

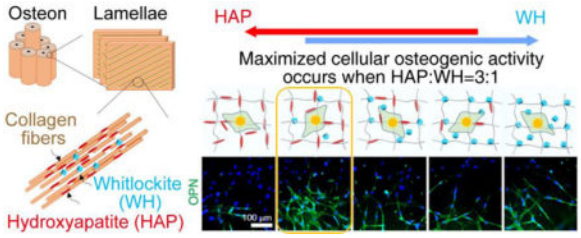

Keywords

bone materials; hydroxyapatite; whitlockite; mesenchymal stem cells; osteogenic differentiation

1. Introduction

One in three people experience bone fractures during their lifetime, in which 10% of cases develop into nonunion fractures. These fractures cannot spontaneously recover, so they require external clinical treatment [1, 2]. To treat nonunion fractures, autologous bone graft transplants are considered a gold standard based on their histocompatibility, as they have similar structure and composition with skeletal tissue around the fracture [3]. However, autografts are limited in supply, require secondary surgery, and can cause morbidity at the donor site [4–6]. Therefore, there have been many attempts to develop bone mimetic materials to substitute the structure and function of autografts. In particular, hydroxyapatite (HAP: $Ca_{10}(PO_4)_6(OH)_2$) bone ceramic materials have been widely investigated and used in the clinic, since it is the major bone mineral in the human body [7–9]. In addition, metallic biomaterials such as titanium, cobalt chrome, stainless steel, and magnesium have been utilized as weight-bearing implants based on their mechanical strength and biocompatibility [10–13]. However, despite recent advances in the field of regenerative medicine, until now there has been no true bone mimetic material that recapitulates the bone niche at the nanoscale, causing a gap between implanted material and the surrounding bone tissues.

At the nanoscale, human bone is composed of collagen fibers, and bone minerals such as HAP and whitlockite (WH: $Ca_{18}Mg_2(HPO_4)_2(PO_4)_{12}$) nanoparticles (Fig. 1a) [14–19]. WH is the second most abundant bone mineral in human body, and occupies approximately up to 25 wt% and 35 wt% of the inorganic portion of human bone and tooth, respectively (Fig. 1b) [15, 16, 20–26]. However, despite its significant amount in human hard tissue, WH has not been applied to the clinic, largely due to its difficulty in synthesis. The reason for this difficulty is because HAP easily precipitates from calcium ions and phosphate ions at neutral pH, as HAP is one of the most thermodynamically stable calcium phosphate compounds in physiological conditions. In addition, HAP is a nonstoichiometric compound that allows for large disruptions of its atomic structure [15, 16]. Recently, we found that a pure phase of WH nanoparticles can be precipitated in acidic aqueous system where excessive amounts of Mg^{2+} ions exist. In particular, the stability of HAP becomes lower in acidic pH conditions, and Mg^{2+} ions are too small to maintain the crystal structure of HAP, thus impeding its precipitation [16, 27, 28]. Based on this synthetic method, our group has previously

analyzed the material properties of WH, and demonstrated the superior osteogenic capability of WH compared to HAP in both *in vitro* and *in vivo* [29, 30].

HAP and WH have different atomic arrangements based on their hexagonal ($P6_3/m$) and rhombohedral (R3c) crystal structures, and exhibit different material properties [15, 16]. For example, while HAP has greater stability in neutral pH conditions [30, 31], WH has higher stability in acidic conditions (pH<4.2) [28, 31]. As a result, WH has a higher solubility than HAP in physiological conditions, and can continuously supply ions such as Mg^{2+} or PO_4^{3-} ions that can stimulate ion channels at the membrane of stem cells, and enhance the osteogenic activity of cells [16, 30, 32]. In addition, while HAP has a net neutral surface charge, WH has a negatively charged surface which enables positively charged osteogenic proteins such as bone morphogenetic protein (BMP) to be adsorbed on its surface by electrostatic interactions [30, 33, 34]. Since HAP and WH have different material properties, it is possible that HAP and WH may have different biological roles in human skeletal tissue.

In this study, we hypothesized that HAP and WH composites may induce a synergistic effect on the osteogenic activity of cells, as human bone is composed of HAP and WH, and because composite materials often exhibit improved biocompatibility and tissue regeneration capacity than monophase materials. For example, biphasic calcium phosphate materials composed of HAP and β-tricalcium phosphate (β-TCP: $Ca_3(PO_4)_2$) have better bone formation capacity compared to HAP or β-TCP when they are used alone in both *in vitro* and *in vivo*, probably based on the synergism between HAP and β-TCP to provide a bioactive surface and ion release, respectively [35–37]. In addition, the incorporation of silica-based bioactive glass into calcium phosphate bioceramic materials can accelerate the degradation of the composite material, and improve bone formation *in vivo* [38]. When β-TCP is mixed with β-calcium silicate (β-$CaSiO_3$), new bone formation was significantly enhanced based on their osteoconductivity and bioactivity, respectively [39]. However, until now, there has been no literature that has identified the synergistic effect between the two major bone minerals in human body.

Inspired by human bone, for the first time, we have developed HAP/WH nanocomposite scaffolds that have a compositional analogy with human bone tissue. In particular, we postulated that a 3D cellular microenvironment that is composed of an optimal ratio between HAP and WH could maximize the osteogenic activity of embedded cells *via* a synergistic effect between HAP and WH, due to their different material properties including stability and ion-releasing capacity. To verify our hypothesis, we designed 3D bone-mimetic HAP/WH nanocomposite hydrogel scaffolds with various ratios of HAP and WH to analyze their material properties, and to assess the cellular response (Fig. 1c).

2. Materials and methods

2.1. Synthesis of GelMA macromonomers and preparation of HAP and WH nanoparticles

GelMA macromonomers with ~90% methacrylation degree were prepared according to established protocols [40], using gelatin from porcine skin (gel strength 300, Type A, Sigma-Aldrich) and methacrylic anhydride (94%, Sigma-Aldrich). HAP and WH nanoparticles were synthesized based on a precipitation method in aqueous system, according to the

literature [31]. Lyophilized GelMA macromonomers were fully dissolved in distilled water with different concentrations (5-10% (w/v)). HAP and WH nanoparticles were homogeneously dispersed in distilled water using ultrasonication, and then dispersed into GelMA solution with different concentration (1-1000 μg/ml) and ratio (1:0, 3:1, 1:1, 1:3, 0:1).

2.2. UV photocrosslinking of composite prepolymer solution

0.5% (w/v) of photoinitiator (Irgacure 2959, 98%, Sigma-Aldrich) was added to HAP and WH mixed GelMA prepolymer solutions, and the resulting mixture was homogenized in a sonication bath for 30 min. Certain amounts of the composite prepolymer solution was then transferred into a customized cylindrical mold made of polydimethylsiloxane (PDMS) and covered with a glass coverslip. By exposing to UV light (6.9 mW/cm^2, 360–480 nm) for 30 s, the composite prepolymer solution was photocrosslinked into a hydrogel scaffold.

2.3. Characterization of nanocomposite hydrogel materials

After lyophilizing the nanocomposite hydrogel scaffolds, the samples were coated with a thin conductive layer of Au (~5 nm) using the Sputter Coater. The morphology of composite hydrogel materials was observed by using FESEM (Zeiss Ultra 55) and their chemical components were detected by utilizing Energy-Dispersive X-ray Spectroscopy (EDS) area scan. To analyze the crystal structure of lyophilized nanocomposite hydrogel scaffolds, samples were grinded into powders and XRD (DMAX2400 Rigaku diffractometer) analysis was conducted with the scan rate of 1° min^{-1} with monochromatic Cu KR radiation (λ = 1.5405 Å). Grinded samples were also analyzed with FT-IR (Bruker Vertex 70), to confirm the maintenance of chemical functional groups of each material type after fabrication process.

2.4. Mechanical analysis

Cylindrically shaped composite hydrogel samples with 10 mm diameter and 2 mm height were prepared using a customized PDMS molds. Samples were then incubated in PBS at 37°C for 24 h to reach the equilibrium swelling state. Compression tests were conducted by using the Instron 5542 mechanical tester: the samples were compressed for 30 s at the rate of 1 mm/min. The Young's modulus was obtained from the slope of the initial linear region (0-10%) of the stress-strain curve (n=3).

2.5. Cell encapsulation in composite hydrogel scaffold and viability, proliferation, and spreading analysis

To develop cell-laden scaffolds, 1×10^6 cells/mL of MSCs (Poietics™ Normal Human Bone Marrow Derived Mesenchymal Stem Cells, Lonza, PT-2501) were added into the composite GelMA presolution right before the photocrosslinking step. Cell-laden composite hydrogel samples were then photocrosslinked by 6.9 mW/cm^2 of UV exposure for 30 s, which was the optimized condition that did not induce cell damage (data not shown). These cell-laden samples were then cultured with either general growth medium or osteoinductive medium, respectively. General growth medium was prepared by mixing Dulbecco's modified Eagle's medium (DMEM) with 10% fetal bovine serum (FBS) and 1% penicillin-streptomycin. The

osteoinductive medium was prepared by including L-ascorbic acid (50 μg/mL) and β-glycerol phosphate (10 mM) in general growth medium. MSCs with passage number below 6 were used for the experiments. Media was changed every 3 days.

To evaluate cellular viability, a live/dead assay (Live/Dead® viability/cytotoxicity kit, Thermo Fisher Scientific) was conducted by staining live cells and dead cells with calcein acetoxymethyl (0.5 μL/mL) and ethidium homodimer-1 (EthD-1, 2 μL/mL), respectively. After incubating stained cells at 37°C for 30 min, cells were gently rinsed with PBS three times and observed by an inverted fluorescence microscope (Nikon TE 2000-U, Nikon instruments Inc., US). The number of live cells and dead cells were quantified from at least 3 independent images. Cell viability was calculated from the percent ratio between number of the live cells and the total number of cells. In addition, the cell proliferation rate was determined from cell number counts at day 1, 3 and 7 (n=3). To monitor the spreading behavior of cells that were embedded in composite hydrogel scaffolds, 4′,6-diamidino-2-phenylindole (DAPI) staining and Alexa Fluor® 594 phalloidin staining were conducted to label cellular nuclei and actin, respectively. Samples were treated with 4% (v/v) paraformaldehyde and 0.1% (w/v) Triton™ X-100 solution to fix the embedded cells and increase their permeability, respectively. Non-specific binding sites were blocked by incubating samples in 1% (w/v) bovine serum albumin (BSA, 98%, Sigma-Aldrich) solution. Samples were then incubated in Alexa Fluor 594 phalloidin solution and DAPI solution for 90 min and 10 min, respectively. After thorough PBS rinsing, the spreading behavior of cells were visualized under the confocal microscope and the average cell area was measured by using ImageJ software (n=3).

2.6. RT-PCR experiments and immunostaining

To assess gene expression level related to osteogenic differentiation, RT-PCR was performed with SYBR® Green Supermix (Biorad) and biomarkers related to osteogenesis, including alkaline phosphatase (*ALP*), osteocalcin (*OCN*), osteopontin (*OPN*) and runt-related transcription factor 2 (*RUNX2*). The sequences of the primers that we used in the RT-PCR are: *GAPDH* (forward: 5′-ACAGTTGCCATGTAGACC-3′, reverse: 5′-TTTTTGGTTGAGCACAGG-3′), *ALP* (forward: 5′-GAGTATGAGAGTGACGAGAA-3′, reverse: 5′-AGTGGGAGTGCTTGTATC-3′), *OCN* (forward: 5′-ATGAGAGCCCTCACACTCCTCG-3′, reverse: 5′-GTCAGCCAACTCGTCACAGTCC-3′), *OPN* (forward: 5′-TTCCAAGTAAGTCCAACGAAAG-3′, reverse: 5′-GTGACCAGTTCATCAGATTCAT-3′), *RUNX2* (forward: 5′-CGGAATGCCTCTGCTGTTATGAA-3′, reverse: 5′-ACTCTTGCCTCGTCCACTCC-3′). After two weeks of culturing cell-laden samples in either general growth medium or osteoinductive medium, samples were treated with TRIzol to isolate RNA. Three samples were used for all experimental conditions. To evaluate protein expression levels related to osteogenic differentiation, samples were fixed with 4% (v/v) paraformaldehyde and treated 0.1% (w/v) Triton X-100 solution. Blocking was performed by incubating samples in 4% normal goat serum (abcam) for 30 min. These samples were then incubated with primary antibodies and secondary antibodies at 37°C for 2 h and 1 h, respectively. We used ALP (Santa Cruz Biotechnology sc-271431), OCN (Millipore MABD123), OPN (Millipore

AB1870), and RUNX2 (Millipore 05-1478) antibodies for the immunostaining. Alexa Fluor 594 phalloidin staining and DAPI staining were conducted at the end. The staining images were obtained using an inverted fluorescence microscope, and protein expression was quantified by using ImageJ software, in which the stained area of the experimental group was divided with the control group.

2.7. Statistical Analysis

Experimental data were processed with one-way ANOVA followed by Bonferroni's post hoc analysis (GraphPad Prism 6.0 software) to establish statistical significance. Error bars represented the mean ± standard deviation (SD) of measurements (*$p < 0.05$ and **$p < 0.01$).

3. Results

3.1. Fabrication of HAP and WH nanocomposite GelMA hydrogel scaffolds

To control the composition of bone mimetic scaffolds and its mechanical properties, we prepared nanosized HAP and WH particles (Fig. 2a–b) and gelatin methacryloyl (GelMA) hydrogel scaffolds (Fig. 2c), according to our previous protocols [31, 40]. The GelMA hydrogel was selected as it is derived from collagen, and its mechanical properties are easy to tune by regulating fabrication conditions. We have optimized the stiffness of GelMA hydrogel scaffolds to approximately 20-25 kPa by using 7% GelMA hydrogel and crosslinking it for 30 sec at 6.9 mW/cm UV light (360-480 nm), as this stiffness range provides a suitable niche for bone cell growth [41, 42]. After homogeneously dispersing HAP and WH nanoparticles in GelMA hydrogel scaffolds with different ratios, we were able to observe the presence of needle-shaped HAP nanoparticles and cuboid-shaped WH nanoparticles in the GelMA hydrogel matrix, by field-emission scanning electron microscopy (FESEM) image analysis (Fig. 2d–f). In the FESEM images, GelMA nanocomposite hydrogel scaffolds with 1000 μg/mL of bone minerals were used for their optimal visualization in the hydrogel matrix. X-ray diffraction (XRD) pattern analysis showed that the crystal phase of HAP and WH in hydrogel composite scaffolds matched well with JCPDS references of HAP (JCPDS 84-1998) and WH (JCPDS 70-2064), respectively, showing that HAP and WH remain intact after being incorporated into GelMA solution and crosslinked into a composite scaffold (Fig. 2g). Fourier-Transform Infrared Spectroscopy (FT-IR) data also showed that there was almost no peak shift or broadening of the amide functional groups in the GelMA hydrogels after mixing with nanoparticles, confirming that denaturation had not taken place (Fig. 2h). In addition, maintenance of P-(OH) stretching of WH (917 cm^{-1}) indicated that there was no severe change of chemical groups in WH during composite biomaterial fabrication.

3.2. Mechanical characterization of HAP and WH nanocomposite GelMA hydrogel scaffolds

The Young's modulus of these HAP/WH nanocomposite hydrogel scaffolds were dependent on the concentration of nanoparticles and the ratio between HAP and WH nanoparticles (Fig. 2i). For instance, as the concentration of nanoparticles in the hydrogel scaffold increased from 1 μg/ml to 1000 μg/ml, the stiffness of the HAP/GelMA hydrogel scaffold and WH/GelMA hydrogel scaffold increased from ~23 kPa to ~29 kPa, and from ~18 kPa to

~24 kPa, respectively. Interestingly, when the ratio of HAP to WH was increased, the overall stiffness of the composite hydrogel scaffolds significantly increased, whereas higher ratio of WH nanoparticles decreased the net stiffness of the nanocomposite hydrogel scaffolds. For instance, when 1, 10, and 100 μg/ml of WH nanoparticles were mixed into GelMA hydrogel scaffolds, the stiffness values of the GelMA composite hydrogel scaffolds were counterintuitively decreased to ~18 kPa, ~19 kPa, and ~20 kPa, respectively, compared to pure GelMA hydrogel scaffolds (~23 kPa). As the concentration of WH in the GelMA hydrogels increased to 1000 μg/ml, the stiffness of the composite hydrogel eventually recovered, probably due to the intrinsic hardness of inorganic particles. These results suggest that HAP can provide a mechanically stable microenvironment compared to WH in hydrogel materials.

3.3. Growth of MSCs embedded in HAP and WH nanocomposite GelMA hydrogel scaffolds

To define the optimal concentration of HAP and WH nanoparticles in GelMA hydrogel scaffolds for promoting the growth of cells, we cultured MSCs in HAP/WH GelMA hydrogel scaffolds, and found that 100 μg/ml of bone minerals in GelMA hydrogel scaffold can induce the highest cellular proliferation for both of HAP and WH (Supplementary information, Fig. S1). Therefore, we conducted all other experiments by using 100 μg/ml of bone minerals for the growth of MSCs. We then controlled the ratio between HAP and WH nanoparticles in the GelMA hydrogel scaffold (HAP: WH=1:0, 3:1, 1:1, 1:3, 0:1). Cellular viability was higher than 90% in all composite scaffolds with various ratios of HAP and WH (Fig. 3a–b and Supplementary information, Fig. S2). Proliferation of cells was also increased in all composite scaffolds with different ratios of HAP and WH (Fig. 3c–d). The viability test and proliferation test were conducted on cell-laden scaffolds that were independently cultured in general growth medium and osteoinductive medium. In addition, confocal microscopy demonstrated that cells spread well in all types of the HAP and WH composite scaffolds, while cellular spreading was improved when HAP and WH nanoparticles were mixed in the scaffolds compared to HAP (Fig. 3e–k).

3.4. Osteogenic activity of MSCs embedded in HAP and WH nanocomposite GelMA hydrogel scaffolds

After culturing MSCs in various ratios of HAP and WH incorporated GelMA hydrogel scaffolds for 14 days, we further assessed gene and protein expression level of MSCs related to osteogenic markers, including *ALP, OCN, OPN* and *RUNX2*, by utilizing real time PCR (RT-PCR) and immunostaining (Fig. 4). The rationale for choosing day 14 as a time point for analyzing protein and gene expression of MSCs related to osteogenic markers was because it is the time point at which MSCs differentiate into pre-osteoblasts, while not completely maturing into osteoblasts [43–45]. As such, we intended to distinguish the effect of bone minerals for promoting the differentiation of pre-osteoblasts. Cell-embedded scaffolds were independently cultured in both general growth medium and osteoinductive medium. While WH is known to promote the osteogenic activity of cells more than HAP, notably, the bone forming activity of cells was significantly greater when their microenvironment was composed of HAP and WH in a 3:1 ratio than any other ratios. For example, from the immunostaining images observed under fluorescence microscopy, *ALP*

expression of MSCs grown in a 3:1 ratio of HAP/WH composite scaffolds was 8.45 times higher than HAP scaffolds, and 1.52 times higher than WH scaffolds.

This trend was consistent in the gene expression analysis that was conducted with identical osteogenic markers which were normalized to the GAPDH housekeeping gene, assuring that the 3:1 ratio of HAP and WH could provide the optimal niche for cells to upregulate gene expression that is relevant to bone cell differentiation (Fig. 4c and f). The relative fold increase in transcript levels of cells grown in 3:1 ratio of HAP and WH that was normalized to HAP scaffold was significantly higher compared to that of WH scaffolds, when cells were grown in general cell growth medium. When a similar experiment was independently conducted using osteoinductive medium, the mRNA expression levels among samples had a similar tendency with samples cultured by general cell growth medium. To ensure reproducibility, the entire experimental procedure for growing cells in HAP/WH composite hydrogel scaffold and analyzing their osteogenic gene expression was repeated by an additional researcher as an independent experiment (Supplementary information, Fig. S3).

To analyze how HAP and WH induces synergism for directing the osteogenic differentiation of MSCs, while WH has superior osteogenic capacity than HAP, we paid attention to the fact that HAP nanoparticles can provide a more mechanically stable microenvironment compared to WH nanoparticles in the GelMA hydrogel matrix. To verify the effect of stiffness of GelMA hydrogel scaffolds on the osteogenic activity of embedded cells, we prepared GelMA hydrogel scaffolds with various stiffness conditions (~26 kPa, ~23 kPa, ~19 kPa, ~14 kPa) by regulating UV exposure time (Fig. 5a). The result showed that cellular gene expression related to osteogenic markers significantly increased when the stiffness of the niches increased (Fig. 5b). In this respect, HAP incorporated GelMA hydrogel scaffold generated a more mechanically stable microenvironment for cells compared to WH. This result can explain the reason for the highest osteogenic activity level of cells expressed in HAP and WH composite hydrogel scaffolds, where both advantages of mechanical stability and bioactivity are provided, instead of either a HAP or WH hydrogel scaffold.

Based on these results, we further narrowed the ratio between HAP and WH in the composite hydrogel scaffold near around 3:1, and assessed the osteogenic activity of cells to find their optimal ratio range for bone formation in detail (Fig. 5c). The osteogenic activity of MSCs was maximized when the content of WH was approximately in a range of 15-25% in the inorganic portion of HAP and WH composite hydrogel scaffold, which was surprisingly similar to the ratio of WH in human native bone as illustrated in Fig. 1a.

4. Discussion

We have previously reported a facile method for synthesizing the pure phase of WH nanoparticles in an aqueous system in large quantities [31]. WH nanoparticles are obtained when calcium, magnesium and phosphate ions react in acidic pH conditions, where the stability of HAP is lower than WH. On the other hand, WH exhibits higher solubility than HAP at neutral pH conditions, thereby continuously releasing a greater amount of ions than HAP in physiological conditions. By controlling pH, HAP and WH can transform into each other through dissolution and re-precipitation processes in the long term [28]. However, even

though both HAP and WH are mainly composed of calcium and phosphate ions, these two bone minerals have different crystal structures and physicochemical properties, such as: solubility, surface charge, and mechanical strength [29–31]. For example, while HAP has a higher stability than WH in physiological conditions, WH has superior osteogenic capacity than HAP [29–31]. In this sense, it is reasonable to hypothesize that these two minerals may have distinguished roles for maintaining the health of human skeletal tissues. Therefore, we raised a question as to why HAP and WH co-exist in human bone tissue with a certain ratio, and hypothesized that there may exist a synergism between HAP and WH for promoting bone growth and regeneration.

In this study, we showed that HAP and WH could generate a synergistic effect to promote the growth and osteogenic activity of MSCs when mixed in hydrogel composite scaffolds, compared to scaffolds composed of either HAP or WH. We defined the optimal ratio between HAP and WH to maximize this synergism to about 3 to 1 (wt%) after comparing various samples with different ratios between HAP and WH. Interestingly, this result corresponded well to the ratio of HAP and WH that exists in human bone, as shown in Fig. 1b. This finding is significant since we have recapitulated the human bone niche at the nanoscale by using HAP and WH nanoparticles for the first time, and revealed that human bone may be organized by HAP and WH with a certain ratio that can maximize the osteogenic activity of cells.

We further analyzed the unique physicochemical properties of HAP and WH nanoparticles when they are homogeneously mixed in the hydrogel matrix. Interestingly, while the addition of HAP nanoparticles in GelMA hydrogel scaffolds increased the stiffness of the composite material, the inclusion of low concentrations of WH nanoparticles (<100 μg/ml) decreased the stiffness of the composite material compared to the pure GelMA hydrogel material. This phenomenon indicated that HAP may provide a more stable 3D microenvironment for embedded cells to grow in the 3D composite hydrogel matrix. When the concentration of WH nanoparticles in GelMA hydrogel scaffolds was 1000 μg/ml, the stiffness of the composite material eventually became higher than the pure GelMA hydrogel material, based on the strong intrinsic mechanical strength of bioceramic particles. In fact, the mechanical test results we obtained showed different tendencies from previous studies, which analyzed the mechanical strength of pure HAP and WH bioceramic materials [29]. Previously, the compressive strength of HAP and WH bioceramic scaffolds were measured after they were prepared as cylindrical pellets. Specifically, HAP or WH nanoparticles were filled in a cylindrical metallic mold, compressed at high pressure, and sintered at high temperatures (>700°C). When the scaffolds were solely composed of bioceramic materials, the compressive strength of WH bioceramic scaffolds was higher than HAP bioceramic scaffolds. Based on these facts, we speculate that WH may have disturbed the crosslinking network of the GelMA hydrogel, and decreased the stiffness of the composite hydrogel material.

A possible reason for the decreased stiffness of GelMA hydrogel scaffolds after the incorporation of WH nanoparticles may be due to the negatively charged surface of WH, which could have induced repulsive electrostatic interactions with the carboxylic acid groups in the GelMA hydrogel network. GelMA hydrogel is a gelatin derivative modified by

methacrylic anhydride by the partial substitution of methacryloyl groups on the amine groups of amino acid residues [40]. As a result, GelMA hydrogel has a negative net charge due to the remaining carboxyl groups [46]. In this respect, negatively charged WH nanoparticles could have disturbed the interactions between carboxylic group and amine groups in the gelatin network, and may have reduced the stiffness of the composite hydrogel scaffolds.

Notably, even though the incorporation of WH nanoparticles in the hydrogel scaffolds exhibited lower mechanical stiffness than HAP composite hydrogel scaffolds, MSCs that were grown in WH composite hydrogel scaffolds exhibited a higher level of growth and osteogenic activity. This result matched well with previous *in vitro* and *in vivo* results that showed a superior osteogenic capacity of WH when cells were grown under the presence of nanoparticles or on the surface of bioceramic scaffolds [29, 30]. Among many reasons, WH could directly upregulate the growth and osteogenic differentiation of stem cells by continuous releasing Mg^{2+} ions and PO_4^{3-} ions, and adsorbing osteogenic proteins on its surface [30]. Up to certain concentrations (~5 mM), the addition of Mg^{2+} ions and PO_4^{3-} ions during cell culture can directly upregulate the osteogenic activity of cells [30]. Since the result from the current study showed that the composite hydrogel scaffolds composed of a mixture of HAP and WH in a 3 to 1 ratio maximized the osteogenic differentiation of MSCs, we concluded that both HAP and WH provided beneficial effects for the growth of embedded MSCs. In particular, the addition of HAP in the hydrogel matrix resulted in a more stable microenvironment for osteogenic cells, while WH could directly stimulate their osteogenic activity.

Note that even though WH gradually dissolves in physiological conditions due to its higher solubility than HAP, WH can mostly maintain its material phase, mass, and shape for at least several months both *in vitro* and *in vivo* [29–31]. WH can maintain its crystal phase even in extreme conditions (90°C, pH 12 sodium phosphate buffer) for at least two weeks, where the stability of HAP is much higher than WH [31]. When 10 g of WH was aged in 1 L of distilled water for one month, its phosphate ion releasing level was only ~18 mg/L [30]. In addition, when WH-incorporated chondroitin sulfate cryogel scaffolds were implanted *in vivo* for longer than six months, we monitored that WH maintained its unique rhombohedral morphology. Here, we also observed HAP precipitation, which co-existed with the WH nanoparticles [30]. In this case, new HAP minerals were not formed directly from WH, but were generated from a high concentration of ions *in vivo.* Since our *in vitro* conditions did not include such a high concentration of calcium and phosphate ions, major phase conversions from WH to HAP may not occur within 2 weeks.

Although HAP and WH composite hydrogel scaffolds significantly improved the osteogenic activity of embedded cells, our study has a limitation in that the concentration of bone minerals in hydrogel scaffolds was much lower than human bone. In this respect, the negative effect of WH for disturbing the mechanical stability of the organic matrix may not be significant in native bone. In addition, there may be additional mechanisms that generate synergism between HAP and WH, or different reasons that HAP and WH coexist in human bone tissue. For example, previously, we demonstrated that precipitation of WH can occur in acidic conditions, while HAP generally forms in neutral pH condition. This implies that WH

may form under acidic conditions *in vivo*, which can be locally formed on the surface of bone during the remodeling process when osteoclasts resorb old bone by secreting acidic molecules [47, 48]. Therefore, identification of the exact formation mechanism of WH *in vivo* can be conducted as an interesting future study to reveal other reasons for co-existence of HAP and WH in human bone.

We expect that our HAP and WH composite hydrogel scaffold platform will be useful for the treatment of bone defects as HAP and WH are the identical materials with human bone minerals. In addition, hydrogel based scaffolds not only mimic extracellular matrix of human tissue, but can also improve viable cell engraftments, and allow for the growth of blood vessels and nerve fibers that exist throughout skeletal tissue [49–51]. In fact, the growth of blood vessel and nerve tissues in implants are critical for bone regeneration, as they can supply oxygen, cells, nutrients and hormones, preventing implant failure and tissue necrosis. Furthermore, HAP and WH composite hydrogel scaffolds are resorbable *in vivo*, and can be replaced by native tissues [29]. While both HAP and WH bone materials are resorbable, WH bioceramic implants exhibited faster resorbability than HAP bioceramic implants both *in vitro* and *in vivo* [29, 30]. When mature osteoclasts were grown on the surface of HAP and WH bioceramic scaffolds, the resorbed area of WH bioceramic scaffolds was twice that of HAP bioceramic scaffolds [30]. In addition, when WH bioceramic implants were inserted in a rat calvarial defect model, the resorption rate of WH was faster than HAP, while synthetic HAP had a much slower resorption rate than the regeneration rate of native skeletal tissue, likely due to its high crystallinity [52]. In this respect, the resorbability of the HAP and WH composite hydrogel scaffolds could be controlled by changing the ratio between HAP and WH. GelMA hydrogel material (GelMA concentration<15%, Compressive modulus<~100 kPa) can be also completely degraded in collagenase solution within two months, while its degradability can be tuned depending on its composition and mechanical properties [53]. Taken together, our HAP and WH composite hydrogel scaffolds can act as a biomimetic substitute for supporting the restoration of the structure and function of damaged bone tissue.

5. Conclusion

This study is scientifically important because it determined optimal ratio between HAP and WH in composite hydrogel scaffolds for promoting growth and osteogenic activity of stem cells. Notably, our optimal ratio range between HAP and WH in composite hydrogel scaffolds was around 3 to 1, which was similar to the compositional ratio of native bone tissue. We explored the synergistic mechanism between HAP and WH, and concluded that HAP supported the mechanical stability of composite hydrogel scaffolds, while WH improved the osteogenic capacity of the organic/inorganic hybrid composite scaffold. We expect that this research will contribute to studies for developing bone mimetic materials, and understanding the structure and function of bone components, particularly related to the necessity of the presence of the two minerals in bone. We also anticipate that the recapitulation of bone at the nanoscale will be useful for effective regeneration of damaged/diseased bone in the clinic.

Supplementary Material

Refer to Web version on PubMed Central for supplementary material.

Acknowledgments

This work was supported by the National Institutes of Health (AR057837, AR070647).

References

1. Einhorn TA. Enhancement of fracture-healing. J Bone Joint Surg. 1995; 77:940–956. [PubMed: 7782368]
2. Meisinger C, Wildner M, Stieber J, Heier M, Sangha O, Döring A. Epidemiology of limb fractures. Orthopade. 2002; 31:92–99. [PubMed: 11963475]
3. Amini AR, Laurencin CT, Nukavarapu SP. Bone tissue engineering: Recent advances and challenges. Crit Rev Biomed Eng. 2012; 40:363–408. [PubMed: 23339648]
4. Calori GM, Colombo M, Mazza E, Ripamonti C, Mazzola S, Marelli N, Mineo GV. Monotherapy vs. polytherapy in the treatment of forearm non-unions and bone defects. Injury. 2013; 44:S63–S69. [PubMed: 23351875]
5. Rao RR, Stegemann JP. Cell-based approaches to the engineering of vascularized bone tissue. Cytotherapy. 2013; 15:1309–22. [PubMed: 23999157]
6. Ollivier M, Gay AM, Cerlier A, Lunebourg A, Argenson JN, Parratte S. Can we achieve bone healing using the diamond concept without bone grafting for recalcitrant tibial nonunions? Injury. 2015; 46:1383–1388. [PubMed: 25933808]
7. Hannig M, Hannig C. Nanomaterials in preventive dentistry. Nat Nanotechnol. 2010; 5:565–569. [PubMed: 20581832]
8. Cölfen H. Biomineralization: a crystal-clear view. Nat Mater. 2010; 9:960–961. [PubMed: 21102512]
9. Jackson SF, Randall J. The fine structure of bone. Nature. 1956; 178:798–798.
10. Long M, Rack H. Titanium alloys in total joint replacement-a materials science perspective. Biomaterials. 1998; 19:1621–1639. [PubMed: 9839998]
11. Geetha M, Singh A, Asokamani R, Gogia A. Ti based biomaterials, the ultimate choice for orthopaedic implants-a review. Prog Mater Sci. 2009; 54:397–425.
12. Castellani C, Lindtner RA, Hausbrandt P, Tschegg E, Stanzl-Tschegg SE, Zanoni G, Beck S, Weinberg AM. Bone-implant interface strength and osseointegration: Biodegradable magnesium alloy versus standard titanium control. Acta Biomater. 2011; 7:432–440. [PubMed: 20804867]
13. Chen Q, Thouas GA. Metallic implant biomaterials. Mater Sci Eng R Rep. 2015; 87:1–57.
14. Nair AK, Gautieri A, Chang SW, Buehler MJ. Molecular mechanics of mineralized collagen fibrils in bone. Nat Commun. 2013; 4:1724. [PubMed: 23591891]
15. Elliott, JC. Structure and chemistry of the apatites and other calcium orthophosphates. Elsevier Science & Technology; Amsterdam: 1994.
16. Driessens, FCM., Verbeeck, RMH. Biominerals. CRC Press; Boca Raton: 1990.
17. Scotchford CA, Vickers M, Ali SY. The isolation and characterization of magnesium whitlockite crystals from human articular cartilage. Osteoarthritis Cartilage. 1995; 3:79–94. [PubMed: 7584321]
18. Hayashi Y. High-resolution electron microscopy of mineral deposits on a thin layer of pellicle adhering to intact enamel surface. J Electron Microsc. 1996; 45:501–504.
19. Palamara J, Phakey P, Rachinger W, Orams H. Electron microscopy of surface enamel of human unerupted and erupted teeth. Arch Oral Biol. 1980; 25:715–725. [PubMed: 6943991]
20. Gabriel S. Chemische Untersuchungen über die Mineralstoffe der Knochen und Zähne, Hoppe-Seyler's Z. Physiol Chem. 1894; 18:257–303.
21. Breibart S, Lee JS, McCoord A, Forbes GB. Relation of age to radiomagnesium e change in bone. Exp Biol Med. 1960; 105:361–363.

22. Woodard HQ. The elementary composition of human cortical bone. Health Phys. 1962; 8:513–517. [PubMed: 14001769]
23. Duckworth J, Hill R. The storage of elements in the skeleton. Nutr Abstr Rev. 1953; 23:1–17. [PubMed: 13037142]
24. Zipkin, I. The inorganic composition of bones and teeth, Biological calcification: cellular and molecular aspects. Springer; Boston: 1970. p. 69-103.
25. Long, C., King, J., Sperry, WM. Biochemists' Handbook. Spon Ltd.; London: 1961.
26. Carlstrom D. X-ray crystallographic studies on apatites and calcified structures. Acta Radiol Supplementum. 1955; 121:1.
27. Terpstra RA, Driessens FCM. Magnesium in tooth enamel and synthetic apatites. Calcif Tissue Int. 1986; 39:348–354. [PubMed: 3102026]
28. Jang HL, Lee HK, Jin K, Ahn HY, Lee HE, Nam KT. Phase transformation from hydroxyapatite to the secondary bone mineral, whitlockite. J Mater Chem B. 2015; 3:1342–1349.
29. Jang HL, Zheng GB, Park J, Kim HD, Baek HR, Lee HK, Lee K, Han HN, Lee CK, Hwang NS. In vitro and in vivo evaluation of whitlockite biocompatibility: Comparative study with hydroxyapatite and β-tricalcium phosphate. Adv Healthcare Mater. 2016; 5:128–136.
30. Kim HD, Jang HL, Ahn HY, Lee HK, Park J, Lee ES, Lee EA, Jeong YH, Kim DG, Nam KT. Biomimetic whitlockite inorganic nanoparticles-mediated in situ remodeling and rapid bone regeneration. Biomaterials. 2017; 112:31–43. [PubMed: 27744219]
31. Jang HL, Jin K, Lee J, Kim Y, Nahm SH, Hong KS, Nam KT. Revisiting whitlockite, the second most abundant biomineral in bone: Nanocrystal synthesis in physiologically relevant conditions and biocompatibility evaluation. ACS nano. 2013; 8:634–641. [PubMed: 24299655]
32. Yoshizawa S, Brown A, Barchowsky A, Sfeir C. Role of magnesium ions on osteogenic response in bone marrow stromal cells. Connect Tissue Res. 2014; 55:155–159. [PubMed: 25158202]
33. Wozney JM. Bone morphogenetic proteins. Prog Growth Factor Res. 1989; 1:267–280. [PubMed: 2491264]
34. Rodriguez-Lorenzo L, Vallet-Regı M, Ferreira J. Colloidal processing of hydroxyapatite. Biomaterials. 2001; 22:1847–1852. [PubMed: 11396889]
35. Arinzeh TL, Tran T, Mcalary J, Daculsi G. A comparative study of biphasic calcium phosphate ceramics for human mesenchymal stem-cell-induced bone formation. Biomaterials. 2005; 26:3631–3638. [PubMed: 15621253]
36. Arinzeh TL, Peter SJ, Archambault MP, Van Den Bos C, Gordon S, Kraus K, Smith A, Kadiyala S. Allogeneic mesenchymal stem cells regenerate bone in a critical-sized canine segmental defect. J Bone Joint Surg. 2003; 85:1927–1935. [PubMed: 14563800]
37. Kadiyala S, Jaiswal N, Bruder SP. Culture-expanded, bone marrow-derived mesenchymal stem cells can regenerate a critical-sized segmental bone defect. Tissue Eng. 1997; 3:173–185.
38. Renno A, Van de Watering F, Nejadnik M, Crovace M, Zanotto E, Wolke J, Jansen J, Van Den Beucken J. Incorporation of bioactive glass in calcium phosphate cement: An evaluation. Acta Biomater. 2013; 9:5728–5739. [PubMed: 23159565]
39. Wang C, Xue Y, Lin K, Lu J, Chang J, Sun J. The enhancement of bone regeneration by a combination of osteoconductivity and osteostimulation using ß-$CaSiO_3$/ß-$Ca_3(PO_4)_2$ composite bioceramics. Acta Biomater. 2012; 8:350–360. [PubMed: 21925627]
40. Yue K, Trujillo-de Santiago G, Alvarez MM, Tamayol A, Annabi N, Khademhosseini A. Synthesis, properties, and biomedical applications of gelatin methacryloyl (GelMA) hydrogels. Biomaterials. 2015; 73:254–271. [PubMed: 26414409]
41. Huebsch N, Arany PR, Mao AS, Shvartsman D, Ali OA, Bencherif SA, Rivera-Feliciano J, Mooney DJ. Harnessing traction-mediated manipulation of the cell/matrix interface to control stem-cell fate. Nat Mater. 2010; 9:518–526. [PubMed: 20418863]
42. Engler AJ, Sen S, Sweeney HL, Discher DE. Matrix elasticity directs stem cell lineage specification. Cell. 2006; 126:677–689. [PubMed: 16923388]
43. Paiva KB, Granjeiro JM. Matrix metalloproteinases in bone resorption, remodeling, and repair. Prog Mol Biol Transl Sci. 2017; 148:203–303. [PubMed: 28662823]

44. Safadi, FF., Barbe, MF., Abdelmagid, SM., Rico, MC., Aswad, RA., Litvin, J., Popoff, SN. Bone structure, development and bone biology. In: Khurana, JS., editor. Bone Pathology. Humana Press; 2009. p. 1-50.
45. Kulterer B, Friedl G, Jandrositz A, Sanchez-Cabo F, Prokesch A, Paar C, Scheideler M, Windhager R, Preisegger KH, Trajanoski Z. Gene expression profiling of human mesenchymal stem cells derived from bone marrow during expansion and osteoblast differentiation. BMC genomics. 2007; 8:1–15. [PubMed: 17199895]
46. Zhou L, Tan G, Tan Y, Wang H, Liao J, Ning C. Biomimetic mineralization of anionic gelatin hydrogels: effect of degree of methacrylation. RSC Adv. 2014; 4:21997–22008.
47. Teitelbaum SL. Bone resorption by osteoclasts. Science. 2000; 289:1504–1508. [PubMed: 10968780]
48. Silver I, Murrills R, Etherington D. Microelectrode studies on the acid microenvironment beneath adherent macrophages and osteoclasts. Exp Cell Res. 1988; 175:266–276. [PubMed: 3360056]
49. Burdick JA, Mauck RL, Gerecht S. To serve and protect: hydrogels to improve stem cell-based therapies. Cell stem cell. 2016; 18:13–15. [PubMed: 26748751]
50. Chen YC, Lin RZ, Qi H, Yang Y, Bae H, Melero-Martin JM, Khademhosseini A. Functional human vascular network generated in photocrosslinkable gelatin methacrylate hydrogels. Adv Funct Mater. 2012; 22:2027–2039. [PubMed: 22907987]
51. Marrella A, Lee TY, Lee DH, Karuthedom S, Syla D, Chawla A, Khademhosseini A, Jang HL. Engineering vascularized and innervated bone biomaterials for improved skeletal tissue regeneration. Mater Today. 2017
52. Maxian SH, Zawadsky JP, Dunn MG. Mechanical and histological evaluation of amorphous calcium phosphate and poorly crystallized hydroxyapatite coatings on titanium implants. J Biomed Mater Res Part B. 1993; 27:717–728.
53. Zhao X, Lang Q, Yildirimer L, Lin ZY, Cui W, Annabi N, Ng KW, Dokmeci MR, Ghaemmaghami AM, Khademhosseini A. Photocrosslinkable gelatin hydrogel for epidermal tissue engineering. Adv Healthc Mater. 2016; 5:108–118. [PubMed: 25880725]

Statement of significance

Human bone minerals are composed of HAP and WH inorganic nanoparticles which have different material properties. However, the reason for the coexistence of HAP and WH in human bone is not fully identified, and HAP and WH composite biomaterial has not been utilized in the clinic. In this study, for the first time, we have developed bone mimetic HAP and WH nanocomposite hydrogel scaffolds with various ratios. Importantly, we found out that HAP can more promote the mechanical stiffness of the composite hydrogel scaffolds while WH can more enhance the osteogenic activity of stem cells, which together induced synergism to maximize osteogenic differentiation of stem cells when mixed into 3 to 1 ratio that is similar to human bone.

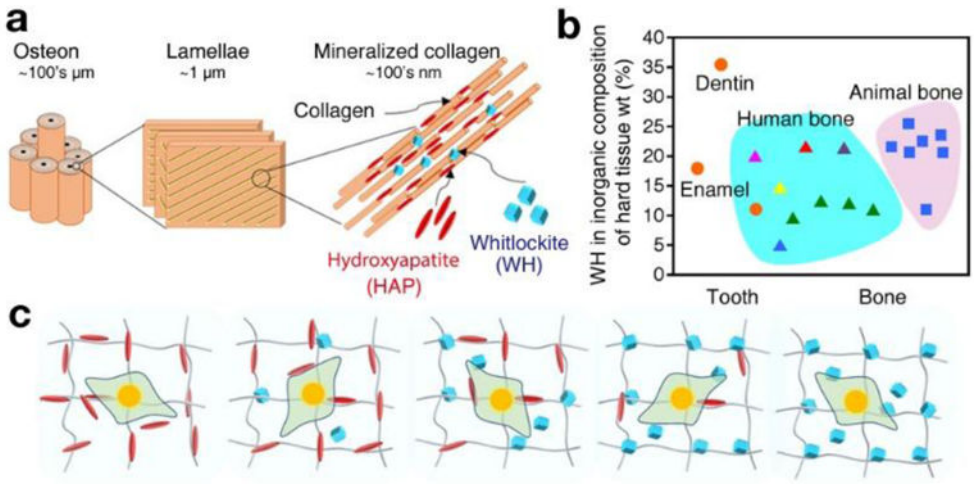

Fig. 1.

The two major inorganic components of bone: hydroxyapatite (HAP: $Ca_{10}(PO_4)_6(OH)_2$) and whitlockite (WH: $Ca_{18}Mg_2(HPO_4)_2(PO_4)_{12}$) nanocrystallites. a) Schematic of bone structure ranging from the nanometer to micrometer scales, showing that bone tissue consists of cylindrical osteon units at the microscale, which are composed of collagen nanofibers with HAP and WH bone mineral particles at the nanoscale. b) Amount (weight percent) of WH in the inorganic part of hard tissues, calculated based on the magnesium amount. Data were obtained from previous publications, with different colors representing different references (Orange circle: Driessens *et al.* [16], Magenta triangle: Gabriels *et al.* [10], red triangle: Carlstrom *et al.* [16], purple triangle: Breibart *et al.* [11], blue triangle: Wooddard *et al.* [12], yellow triangle: Duckworth *et al.* [13], green triangle: Schraer *et al.* [14], blue rectangle: Long *et al.* [15] c) Schematic of experiments to identify optimal conditions in the stem cell niche for osteogenic differentiation of human mesenchymal stem cells (MSCs) with regard to the different ratios of HAP and WH.

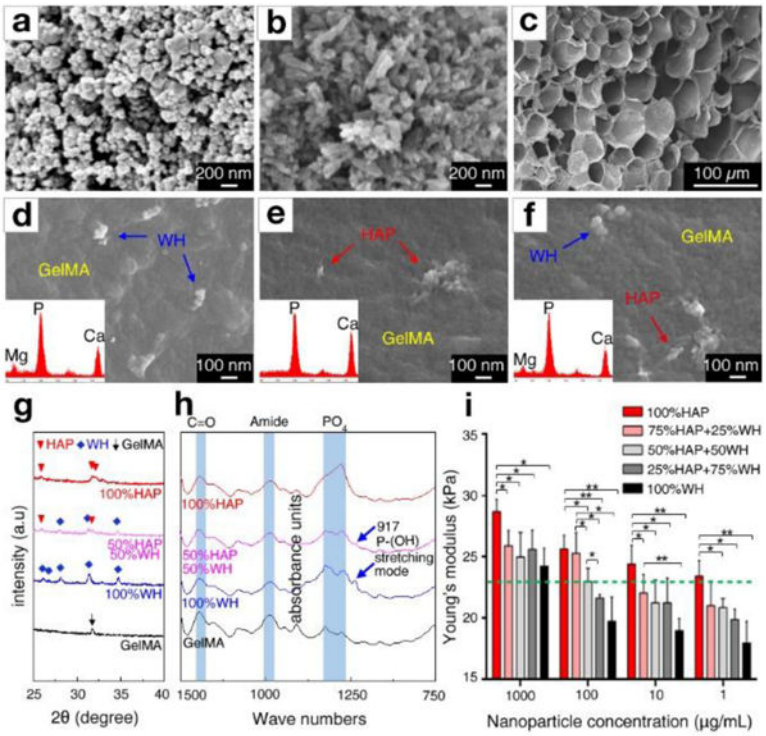

Fig. 2.

Engineered bone-mimetic nanocomposite hydrogel scaffolds. FESEM observation of a) synthesized WH nanoparticles with rhombohedral shape, b) HAP nanoparticles with needle shape, and c) microporous structured GelMA hydrogel scaffold after freeze drying. d-f) The nanoscale features of composite hydrogel scaffolds, showing that rhombohedral shaped WH nanoparticles and needle-shaped HAP nanoparticles are homogeneously dispersed in the GelMA hydrogel. Insets in each panels show the EDS area scan analysis, where WH incorporated GelMA hydrogel had a Mg peak, and HAP incorporated GelMA exhibited a higher ratio of the Ca and P peak intensity. g) XRD analysis of HAP-incorporated GelMA hydrogel and WH-incorporated GelMA hydrogel, confirming that their crystal phase is maintained after fabrication. h) FT-IR analysis result of HAP-incorporated GelMA hydrogel and WH-incorporated GelMA hydrogel, confirming that the chemical groups of HAP, WH and GelMA hydrogel remain intact after fabrication. i) The Young's modulus of the composite hydrogel scaffolds depending on different concentrations and ratios of HAP and WH in GelMA hydrogel were calculated from compression tests. The green dotted line indicates the stiffness of pure GelMA hydrogel (~23 kPa). (*$p<0.05$, **$p<0.01$)

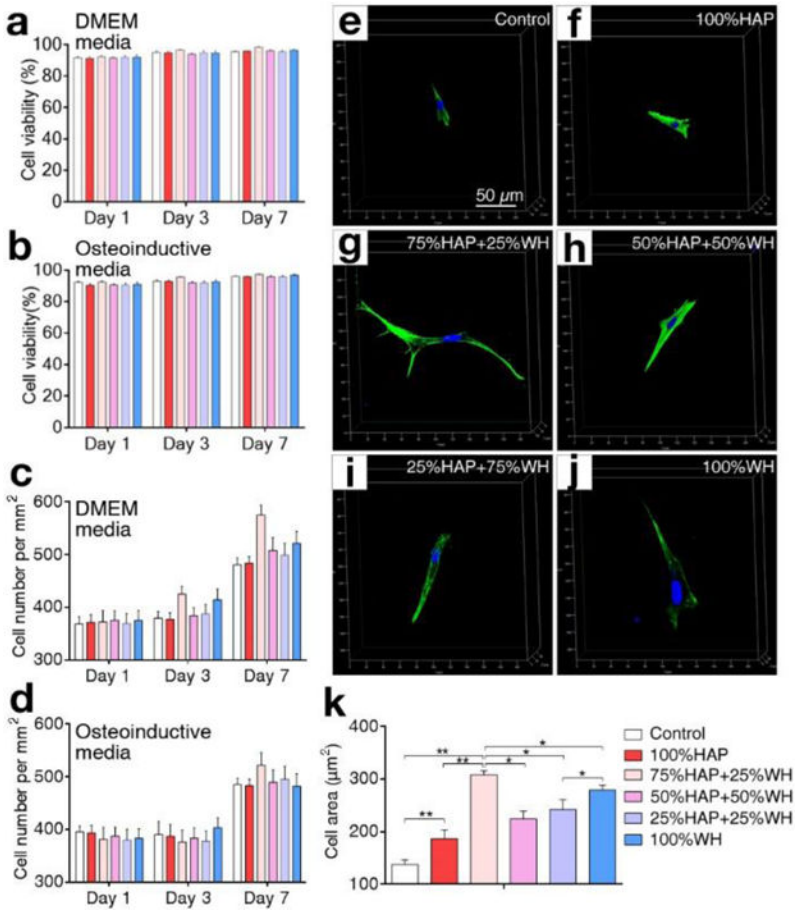

Fig. 3.

Cellular viability, proliferation, and spreading in composite hydrogel scaffolds with different ratios of HAP and WH. a–d) Viability (a–b) and proliferation (c–d) of cells grown in 3D composite hydrogel scaffolds with different ratios of HAP and WH, in two media conditions (DMEM and osteoinductive media) were compared. e–k) Spreading of cells in 3D composite hydrogel scaffolds depending on different ratios of HAP and WH at day 7 was observed under confocal microscopy and quantified based on their spreading area. Cellular nuclei and actin were stained with DAPI (blue) and phalloidin (green). (*$p<0.05$, **$p<0.01$)

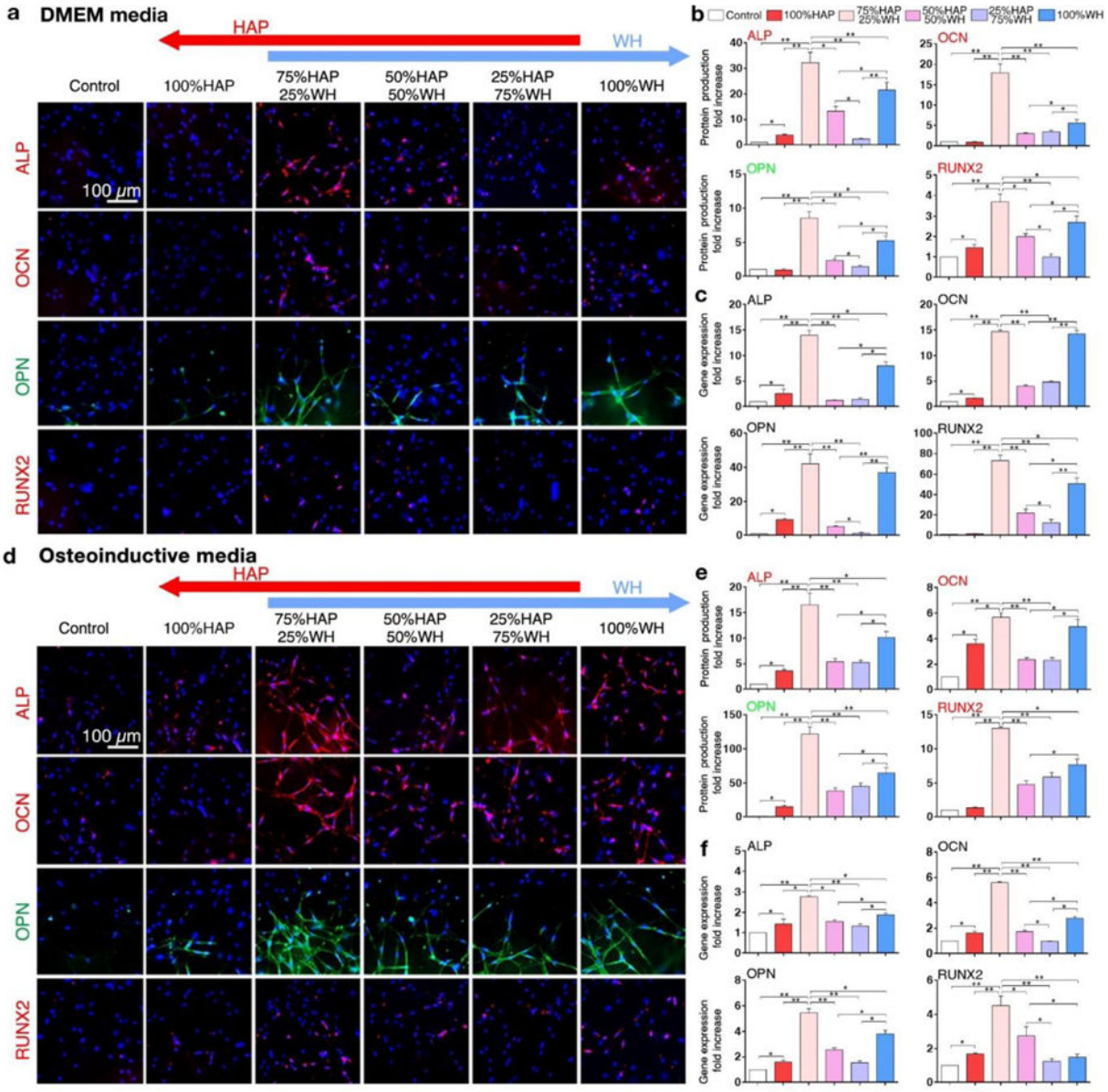

Fig. 4.

Effect of ratios between HAP and WH on osteogenic activity of MSCs that are encapsulated in bone mimetic 3D HAP/WH nanocomposite hydrogel scaffolds. a) Fluorescence images of immunostained MSCs encapsulated in 3D composite hydrogel scaffolds with different ratio of HAP and WH. Osteogenic marker expression of MSCs *(ALP, OCN, OPN, RUNX2)* were compared after grown in DMEM media conditions for 2 weeks. b) Osteogenic protein expression levels of MSCs in panel a were quantified by using ImageJ software and dividing the area of stained images of experimental groups by control groups. The result indicated that cells grown in scaffolds with HAP and WH nanoparticles which were mixed in a 3 to 1 ratio had the highest level of osteogenic gene expression. c) Relative osteogenic gene expressions of MSCs were evaluated by real-time quantitative PCR analysis and calculated by $2^{-\Delta\Delta Ct}$ method, after 2 weeks of culturing in 3D composite hydrogel scaffolds. d)

Fluorescence images of immunostained MSCs that were grown in 3D composite hydrogel scaffolds with different ratio of HAP and WH for 2 weeks under osteoinductive media conditions. e) Quantified osteogenic protein expression levels of MSCs from panel d, based on the same calculation method as mentioned above. f) Relative osteogenic gene expression of MSCs that were cultured in 3D HAP/WH composite hydrogel scaffold for 2 weeks under osteogenic media conditions. (*$p<0.05$, **$p<0.01$)

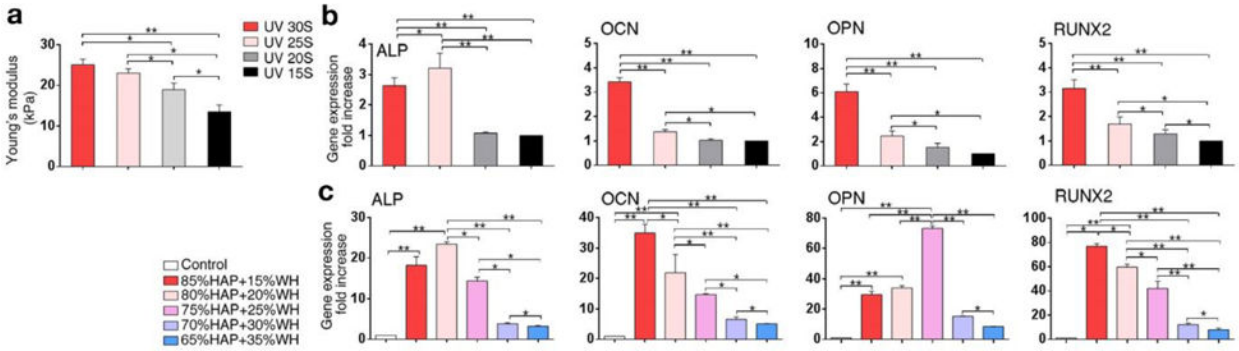

Fig. 5.

Effect of stiffness of composite hydrogel scaffold and the optimal ratio between HAP and WH for directing osteogenic differentiation of MSCs. a) Stiffness of GelMA hydrogel scaffold was tuned by controlling UV exposure time, to assess the effect of the scaffold stiffness on the osteogenic activity of cells grown in it. b) Relative osteogenic gene expression of MSCs cultured in 3D GelMA hydrogel scaffolds with different stiffness level showed that cellular osteogenic activity was generally enhanced as the stiffness of hydrogel scaffold increased, in a range of 13-26 kPa. c) Optimal ratio between HAP and WH for inducing osteogenic differentiation of MSCs was obtained in a narrowed range of 65%HAP +35%WH to 85%HAP+15%WH, by using quantitative real-time PCR. The result showed that the osteogenic activities of cells were more upregulated when the ratio between HAP and WH is in a range of 75%HAP+25%WH to 85%HAP+15%WH. (*p<0.05, **p<0.01)